

Article

Arctic Atmospheric Ducting Characteristics and Their Connections with Arctic Oscillation and Sea Ice

Ting Qin ^{1,2,3,*} , Bo Su ^{3,*}, Li Chen ³, Junfeng Yang ⁴, Hulin Sun ³, Jing Ma ³ and Wenhao Yu ³

¹ State Key Laboratory of Severe Weather, Institute of Tibetan Plateau Meteorology, Chinese Academy of Meteorological Sciences, Beijing 100081, China

² University of Chinese Academy of Sciences, Beijing 100049, China

³ National Marine Environmental Forecasting Center, Beijing 100081, China

⁴ State Key Laboratory of Space Weather, National Space Science Center, Chinese Academy of Sciences, Beijing 100190, China

* Correspondence: tingqin_123@126.com (T.Q.); bosu@nmefc.cn (B.S.)

Abstract: Atmospheric ducting is an anomalous atmospheric structure that affects electromagnetic wave propagation. In the context of global warming, the navigation capacity of the Arctic is increased, and the atmospheric duct can affect communication and navigation in the Arctic. In this study, based on the European Centre for Medium-Range Weather Forecasts reanalysis data (ERA-interim), the climate characteristics and their variations of atmospheric ducts over the Arctic polar region (north of 60° N) from 1989 to 2018 were analyzed, including the occurrence frequency, spatial distribution, thickness and intensity of the atmospheric ducts. The results show that the overall frequency of atmospheric ducts in the Arctic is low, with the average frequency of all types of ducts being less than 10% throughout the year. The frequency of surface ducts is 2~3 times that of elevated ducts. More than 90% of the atmospheric ducts in the Arctic have a trapped layer with a thickness of less than 100 m, and the average thickness of surface ducts is higher than that of the elevated ducts. The intensity of the Arctic surface ducts is stronger than that of the elevated ducts, with an average intensity of 2.1 M (± 2.3 M) to 4.5 M (± 4.5 M) for the surface ducts and 1.7 M (± 2 M) to 2.5 M (± 2.9 M) for the elevated ducts. There is a positive correlation between the ducts' trapped layer thickness and duct intensity. The variation in atmospheric ducts is responsive to the changes in atmospheric circulation and the sea ice extent. This anomalous circulation changes surface wind in the Arctic, which affects the formation and maintenance of the ducts. The trends of ducts in the Arctic Ocean are consistent with those of the Arctic Sea ice extent, while the Arctic continental and coastal ducts show the opposite trend.

Keywords: Arctic atmosphere ducts; spatial and temporal distribution; trapping layer thickness; intensity of ducts; Arctic oscillation; sea ice extent; variation and influence factor analysis



Citation: Qin, T.; Su, B.; Chen, L.; Yang, J.; Sun, H.; Ma, J.; Yu, W. Arctic Atmospheric Ducting Characteristics and Their Connections with Arctic Oscillation and Sea Ice. *Atmosphere* **2022**, *13*, 2119. <https://doi.org/10.3390/atmos13122119>

Academic Editors: Vladimir Ivanov and Zhiping Wen

Received: 13 October 2022

Accepted: 14 December 2022

Published: 16 December 2022

Publisher's Note: MDPI stays neutral with regard to jurisdictional claims in published maps and institutional affiliations.



Copyright: © 2022 by the authors. Licensee MDPI, Basel, Switzerland. This article is an open access article distributed under the terms and conditions of the Creative Commons Attribution (CC BY) license (<https://creativecommons.org/licenses/by/4.0/>).

1. Introduction

Arctic atmospheric ducts can trap electromagnetic waves due to the inhomogeneous atmospheric refractive index, and affect communications and radar detection signals beyond the visible range. Climate and environmental changes in the Arctic have a direct impact on the world, while the reduction of Arctic Sea ice further aggravates global warming through the ice radiation feedback mechanism. The melting of glacial permafrost will bring ecological and economic damage to countries near the polar circle [1,2], which has encouraged an increasing number of scientists to explore Arctic sailing routes and seek their commercial value [3,4]. Many countries have deployed various unmanned scientific research equipment in the Arctic, most of which relies on radio and satellite signals [5–7]. These trends will increase the demand for marine navigation and communication technologies in the Arctic. Therefore, the Arctic atmospheric duct, as a special weather process that affects polar communication signals, is worthy of in-depth analysis.

Atmospheric ducts are triggered by two kinds of atmospheric conditions, one in which atmospheric humidity decreases sharply with height, and the other in which the atmospheric temperature increases with height [8]. The calculation of the atmospheric refractive index can achieve the qualitative analysis of atmospheric ducts. The temperature, humidity and pressure from the ground to the stratosphere must be provided.

The study of ducting characteristics by GPS atmospheric sounding is mainly aimed at regions with data observation. Patterson [9] used global radiosonde measurements to study atmospheric ducts' distribution patterns related radiosonde sites around the world throughout a period of six years, and Babin [10] used helicopter measurements to analyze the seasonal variations of surface ducts located on Wallops Island, Virginia. Lang [11] studied the ducts of the American mainland and found that the precipitation correlates positively with the probability of ducts caused by the vertical moisture gradient, while the relation is negative when the ducts are caused by temperature inversion. Yan [12] focused on the ducts in Alaska and found the Arctic vortex area and intensity index were significantly negatively correlated with the occurrence of atmospheric ducts. The characteristics of atmospheric ducts in the offshore and coastal areas of China have been analyzed using ship-based GPS and shore-based GPS sounding [13–16]. With the use of atmospheric numerical models, research on local and global ducting characteristics is gradually enriched. Chen [17] pointed out that ducts in offshore China exhibit obvious seasonal variations, based on the mesoscale weather numerical model MM5 (Fifth Generation Penn State/NCAR Mesoscale Model). Cheng et al. [18] used ERA-Interim to analyze the characteristics of low-altitude ducts in offshore China, and showed that the overall atmospheric duct frequency was 22%. The characteristics of global atmospheric ducts have been analyzed, including the basic characteristics of the seasonal variation of ducting frequency and thickness [8,19]. It has also been proved that the reanalysis data can accurately reflect the characteristics of atmospheric ducting.

Due to the lack of observational data, the study of the Arctic ducts is still less intensive than that of other regions. Recent research shows that the frequency of atmospheric ducting in the Arctic is significantly lower than that in other sea areas of the world, with an incidence of less than 50% [8,19]. Although previous studies have researched the Arctic [20], the research area is still relatively limited and the time span is still short, given that only 10-year data from 16 stations along the coast of the Arctic continent were analyzed, while the basic statistical characteristics of the ducts, such as strength and height, are not sufficiently clear.

Weather systems and ocean processes, such as blocking highs, polar cyclones, low-level ocean jets and the North Atlantic Current, which trigger moisture inversion, the subsidence of air masses and the passing of cold air over warm land, lead to differences in the frequency, height and intensity of atmospheric ducts [21–27]. However, there have been few studies on the relationship between atmospheric ducting and large-scale atmospheric circulation, especially in the Arctic region.

ERA-Interim reanalysis data of 60 vertical layers with a horizontal resolution of $0.75^\circ \times 0.75^\circ$ were used in this research. This dataset can capture the shape of the mean temperature, wind speed and specific humidity profiles well in the Arctic [28–30]. GPS sounding data in the Arctic Ocean obtained during the sixth to ninth Chinese Arctic scientific expeditions (held in 2014, 2016, 2017 and 2018) are provided for comparison with the reanalysis data in Section 3.1. Based on the ERA-Interim data, the climate characteristics of Arctic atmospheric ducts are investigated for the period of 1989–2018 in Section 3.1 to Section 3.3. Additionally, the response of the Arctic atmospheric ducts to atmospheric circulation and sea ice is in Section 3.4. The climatological analysis of the spatial and temporal distribution and intensity of the atmospheric ducts can serve as a reference for both the improvement of the atmospheric duct detection, prediction and diagnosis system, and the further use of atmospheric ducts for the operation of ship-borne radio systems in the Arctic.

2. Data and Methods

2.1. Data

The ERA-Interim data released by the ECMWF (European Centre for Medium-Range Weather Forecasts) were used to perform a climate analysis of the atmospheric ducting characteristics [31,32]. The data assimilation system used is the Integrated Forecast System (IFS) Cy31r2. The system includes a 4-dimensional variational analysis (4D-Var) with a 12 h analysis window. The spatial resolution of the data set is approximately 80 km (T255 spectral, $0.75^\circ \times 0.75^\circ$) on 60 levels from the surface up to 0.1 hPa. The assimilated data include operational observation data, radiosonde data, wind data from reprocessed meteorological satellites, satellite altimeter data and clear sky radiation from geostationary satellites. There are 11 layers below 1000 m at sea: the influence of orography is not considered. Forecasts were provided at 00, 06, 12 and 18 Universal Time.

The Arctic Oscillation (AO) is a large-scale mode of climate variability, and a climate pattern characterized by winds circulating counterclockwise around the Arctic at around 55° N latitude. It is an important climatic index representing the atmospheric circulation in the Arctic region, which can be divided into positive phase and a negative phase [33]. In Section 3.4 the AO index was obtained from the National Oceanic and Atmospheric Administration (<http://www.esrl.noaa.gov/psd/data/climateindices>, accessed on 28 November 2022). The data used in the composite analysis of Section 3.4 were chosen from ERA5, the monthly product (ERA5 monthly averaged data on single levels from 1959 to present), which mainly uses its 500 hPa geopotential height, sea level pressure and wind speed at 10 m. The ERA5 dataset is the latest reanalysis from the European Centre for Medium-Range Weather Forecasts (ECMWF) based on its previous generation ERA-Interim dataset. Compared with the previous ERA-Interim dataset, the ERA5 dataset has longer time coverage, a more accurate data assimilation system and finer spatial resolution [34].

The sea ice extent from NOAA (https://masie_web.apps.nsidc.org/pub/DATASETS/NOAA/G02135/seaice_analysis, accessed on 6 September 2022) is calculated as the areal sum of sea ice covering the ocean where the sea ice concentration (SIC) exceeds a threshold, which is calculated as the sum of all ocean elements having a sea ice concentration of at least 15%.

Due to the lack of comparison and the verification of fixed-point observation data in the Arctic Ocean, the atmospheric profile data of the GPS radiosonde observation [35] during the sixth to ninth Chinese National Arctic Research Expeditions (CHINARE, held in 2014, 2016, 2017 and 2018) were compared with the reanalysis data to ensure that the ERA-Interim data better reflect the characteristics of the atmospheric profile in the Arctic and the reliability of the atmospheric duct results we calculated based on them. The sounding observations were carried out on the vessel XueLong, about 10 m above the sea surface. The observation frequency is two to three times 00 (UTC), 06 (UTC) and 12 (UTC). During the sixth to eighth Arctic expeditions, the Changfeng-CF-06-A radiosonde was used, with temperature and humidity measurement ranges of -90 to 50°C and 0 to 100%, resolutions of 0.1°C and 1%, errors of 0.5°C and 5% and a response time of less than 1.5 s [36]. During the ninth Arctic expedition, the VaisalaRS41 radiosonde was used, with temperature and humidity measurements ranging from -90 to 60°C and 0–100%, resolutions of 0.01°C and 0.1%, errors of 0.2°C and 3%, and a response time of 0.5 s [35].

2.2. Methods

The occurrence of atmospheric ducts is defined by the change in the atmospheric refractive index [37]. When considering the curvature of the ground, the modified atmospheric refractive index is often used to characterize the atmospheric refraction state [18,19], which is a function of atmospheric pressure, temperature and water vapor pressure, as follows:

$$M = \frac{77.6}{T} \left(P + 4810 \frac{e}{T} \right) + 0.157Z \quad (1)$$

In each layer, M represents the corrected atmospheric refractive index (M), P (hPa) denotes the pressure at the full level (https://rda.ucar.edu/datasets/ds627.2/docs/Eta_coordinate/index.html#sec2, accessed on 3 September 2022), E denotes water vapor pressure (hPa), T denotes air temperature (K) and Z represents altitude above the Earth's surface and the sea surface (m). Z shall be converted through geopotential height h to eliminate continental topography.

$$h = \left(\frac{\phi}{g^0}\right)/1000 \quad (2)$$

$$H = (Re \times h)/(Re - h) \quad (3)$$

$$Z = H - Ze \quad (4)$$

ϕ (m^2/s^2) in Equation (2) is geopotential for each level, $g^0 = 9.8 \text{ m/s}^2$. Re (km) in Equation (3) is the radius of the Earth, h (km) is the geopotential height and H (km) is the geometric height. Ze (km) in Equation (4) is the geoid height from the EGM96 Geopotential Model. Note that the actual height of each model level may vary slightly among model grid points because of horizontal variations in virtual temperature and surface pressure [8,38].

Rogers' [39] water vapor pressure formula (Equation (5)) was used to calculate the atmospheric ducts from the reanalysis data, and the modified Tetens equation (Equation (6)) [11,40,41] was used to calculate the water vapor pressure from GPS atmospheric sounding:

$$e = \frac{qP}{\varepsilon + (1 - \varepsilon)q} \quad (5)$$

$$E = 6.112 \exp\left(\frac{17.67t}{t + 243.5}\right) \quad (6)$$

In Equation (5), q represents the specific humidity (kg/kg) of each layer of the atmosphere, ε with a constant value of 0.622. In Equation (6), E is the saturation water vapor pressure (hPa) at temperature T ($^{\circ}\text{C}$).

When the corrected refractive index gradient is negative ($\frac{dM}{dz} < 0$), and an atmospheric duct is determined to be present, then the refractive index of the atmosphere at the bottom of the negative gradient layer is denoted as M_{max} . The height of the bottom of this layer serves as the base of the atmospheric ducts h_{min} , up to a height such that $\frac{dM}{dz} > 0$, at which height the refractive index of the atmosphere is denoted as M_{min} . The height of this layer serves as the top h_{max} ; this layer is called the trapped layer [42]. Meanwhile, several values representing the characteristics of the atmospheric duct can be calculated, including the trapped layer thickness h_t , as shown in Equation (7), and the intensity of the duct, as shown in Equation (8) [20]. It should be noted that the trapped layer thickness of the surface duct represents the top height and thickness of this kind of duct:

$$\text{Trapped layer thickness: } h_t = h_{max} - h_{min} \quad (7)$$

$$\text{Intensity of the ducts: } \Delta M = M_{max} - M_{min} \quad (8)$$

At present, the internationally recognized atmospheric ducts can be divided into three types, according to the shape of the atmospheric refractive index profile and the height [42]: simple surface ducts (Figure 1a), surface ducts with a base layer (Figure 1b) and elevated ducts (Figure 1c). In this study, both surface ducts and surface ducts with a base layer are considered to be surface ducts, and the cases of surface ducts and elevated ducts in the Arctic region are both discussed.

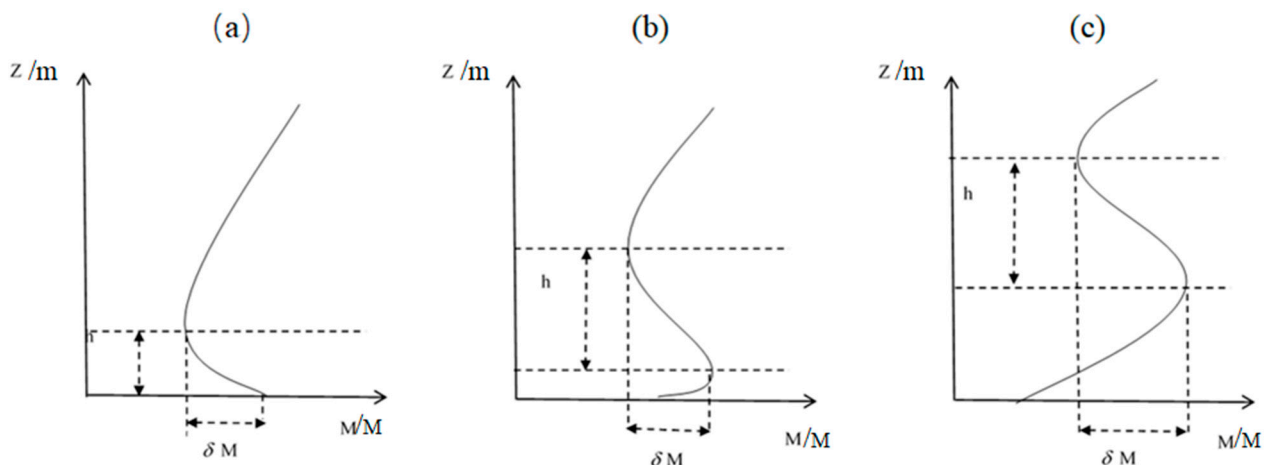


Figure 1. Type diagram of atmospheric duct, where h is the trapped layer thickness and M is the strength: (a) simple surface duct; (b) surface S-shaped duct; (c) elevated duct.

3. Results

3.1. Comparison of GPS Sounding Observations and Reanalysis Data in the Arctic

The occurrence of atmospheric ducting is determined by the modified atmospheric refractive index. In this section, the atmospheric sounding data obtained from the sixth to ninth CHINARE (Figure 2) are evaluated as true values, and the ability of ERA-Interim to calculate the modified atmospheric refractive index is evaluated. The scatter map comparing the modified atmospheric refractive index calculated by ERA-Interim and the GPS atmospheric sounding is shown in Figure 3a. The deviation distribution of the modified atmospheric refractive index with height is given in Figure 3b, and the mean deviation (M.D.) relative deviation (R.D.), Root-Mean-Square Error (RMSE) and median deviation were calculated, as shown in Figure 3b. Among these, the median deviation is the element in the middle of the deviation array after the elements are arranged from small to large, and the other formulas are as follows:

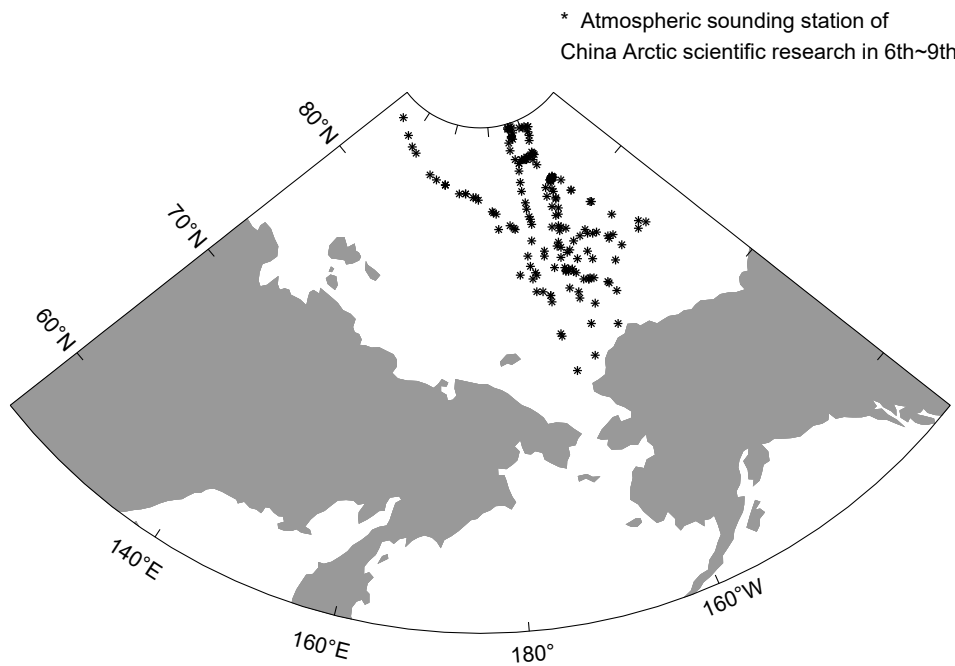
$$M.D. = \left[\sum_{i=1}^n (X_i - Y_i) \right] / n \tag{9}$$

$$R.D. = \sum_{i=1}^n (X_i - Y_i) / \sum_{i=1}^n Y_i \tag{10}$$

$$RMSE = \sqrt{\frac{1}{N-1} \sum_{i=1}^N (x_i - \bar{x})^2} \tag{11}$$

In Equation (7), X_i represents the modified atmospheric refractive index calculated by ERA-Interim, Y_i represents the modified atmospheric refractive index calculated by atmospheric sounding data, n is the number of samples for each layer, x_i is the deviation, \bar{x} is the mean deviation and N is the total samples.

To obtain a better comparison, the modified atmospheric refractive index derived from ERA-interim and GPS atmosphere sounding observation are plotted in Figure 3a. The red dashed line is the regression of the reanalysis data against the observation data. As demonstrated in Figure 3a, the correlation coefficient between them is about 0.982, $r^2 = 0.96$ ($p < 0.05$). This figure illustrates a high linear correspondence between the modified atmospheric refractive index calculated by the reanalysis data and the observation data.



* Atmospheric sounding station of China Arctic scientific research in 6th~9th

Figure 2. Distribution of GPS atmospheric sounding stations during the sixth to ninth CHINARE.

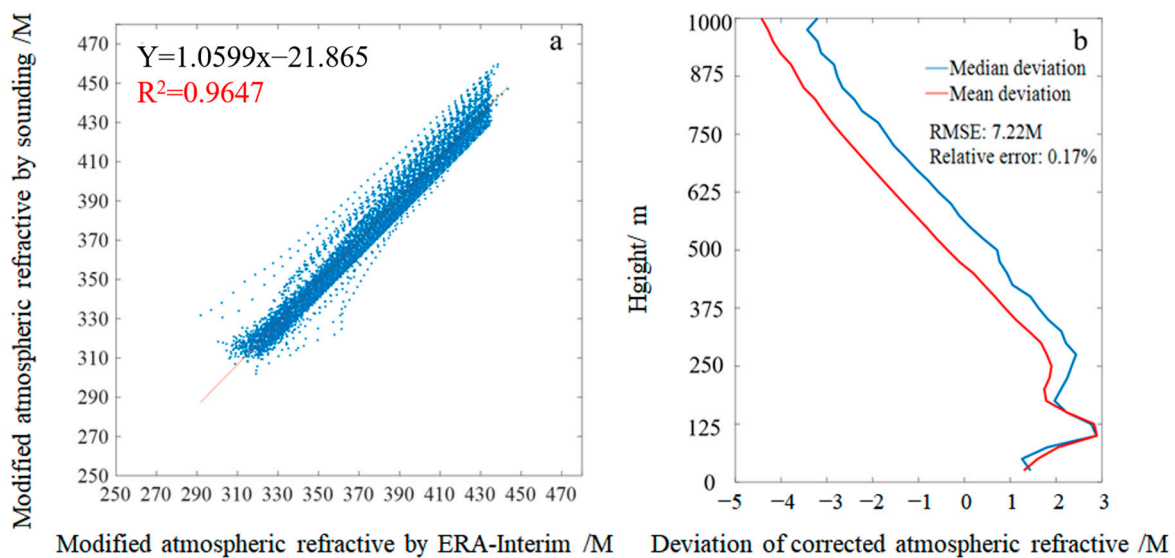


Figure 3. (a) Scatter map comparing the modified atmospheric refractive index calculated by ERA-Interim and the GPS atmospheric sounding; (b) Deviation distribution of modified atmospheric refractive index with height.

Figure 3b shows the statistics of the corrected atmospheric refractive index deviation from the ground to the height of 1000 m. The mean and median deviation have similar distribution curves, indicating that the deviation distribution is symmetrical with the average. The mean deviation range is -3 to 4 M. The mean deviation and median deviation are positive below 500 m, illustrating that the modified atmospheric refractive index calculated from the reanalysis data is higher than that from the observation data, while the opposite is true above 500 m. On the other hand, the distribution of the mean deviation increases sharply with a height below 120 m, and then the average deviation between 120 m and 500 m decreases, while the deviation increases when it is greater than 500 m, but its increase amplitude is smaller than that below 120 m. The mean deviation of 300 m to 600 m is relatively small compared to

those below 200 m and above 600 m, at less than 1 M, and the maximum deviation is -4 M at 1000 m. The RMSE and R.D. are 7.22 M and 0.17%, respectively.

Although deviation occurs when using reanalysis data to calculate the modified atmospheric refractive index at different heights, the ERA-Interim data can accurately reflect the vertical variation characteristics of the index from the significant correlation with the observed data. Therefore, these data can be used to analyze the climatology state of atmospheric ducts in the Arctic. In addition, previous studies [43,44] also show that the data are reliable in describing the vertical characteristics of the atmosphere, and they are also used in the study of atmospheric ducting [19].

3.2. Spatial Characteristics of Atmospheric Duct Frequencies

Next, the spatial distribution and monthly variation of total Arctic ducts are further analyzed. The results in Figure 4 indicate that the occurrence frequency of the Arctic ducts is lower than those of the middle and low latitudes and the Antarctic region, which is consistent with the results of Wang [19]. Duct frequency exhibits significant regional differences. Ducts in the Arctic mainly occur near the coast of the continent, with two high-value regions located between the north of Greenland to the north of Baffin Bay, and the north of Russia between $120\text{--}150^\circ$ E and $60\text{--}70^\circ$ N, near the central Siberian plateau and the Chersky Mountains. The frequency of ducting in the period ranging from winter to early spring on the north coast of Greenland can reach more than 80%, which is much higher than the average of the Arctic. At the same time, the frequency of ducting north of 80° N is lower than that in the lower latitudes, and changes depending on the month, with the frequency in summer being significantly lower than that in other seasons.

Table 1 shows further data statistics, the average frequency of the total ducts throughout the entire Arctic is 4.0–9.9%, of which that of the surface ducts is 2.8–7.3%, and that of the elevated ducts is 1.0–2.6%. The Arctic landmass is mainly located from 60 to 70° N. The average frequency of ducting in this region is 4.4–12.9%, that of the surface ducts is 2.9–8.8%, and that of the elevated ducts is 1.2–4.0%; $70\text{--}80^\circ$ N is mainly the surrounding area of the Arctic Ocean, and has a low sea ice concentration. The average frequency of the total ducts in the $70\text{--}80^\circ$ N region is 3.8–11.8%, that of the surface ducts is 2.0–8.0%, and that of the elevated ducts is 1.3–2.9%; the $80\text{--}90^\circ$ N region has high sea ice concentration area all year round. The total frequency of ducting is 1.2–5.0%, among which that of the surface ducts is 0.6–4.0%, and that of the elevated ducts is 0.5–1.0%.

In winter, the frequency of atmospheric ducts in the $60\text{--}70^\circ$ N region is the highest, which is obviously higher than that in the Arctic Ocean region in the same period, meanwhile, the frequency is obviously more than that in summer. Hao [20] counted the data from three sounding stations in Greenland, and found that 93% of atmospheric duct events in February were accompanied by a thicker radiation inversion layer of the boundary layer, while in summer is 88%. It is speculated that the radiation inversion of the land is the main reason for the formation of the winter ducts. Moreover, the water vapor transported through the Atlantic Warm Current, extratropical cyclone and other processes is blocked in the inversion layer, resulting in a sharp decrease in humidity with height. This can also be seen from the increase in the frequency of the total ducts in winter.

Table 1. Average frequency of atmospheric ducts in different regions of the Arctic.

Parameter	Total Ducts/%				Surface Ducts/%				Elevated Ducts/%			
	Latitude	Spr.	Sum.	Aut.	Win.	Spr.	Sum.	Aut.	Win.	Spr.	Sum.	Aut.
60° N– 70° N	7.1	10.2	4.4	12.9	5.9	7.4	2.9	8.8	1.2	2.9	1.5	4.0
70° N– 80° N	5.7	3.8	4.9	11.8	4.5	2.0	3.3	8.8	1.3	1.8	1.6	2.9
80° N– 90° N	3.1	1.2	2.7	5.0	2.6	0.6	2.1	4.0	0.5	0.6	0.5	1.0
Total	5.3	5.1	4.0	9.9	4.3	3.3	2.8	7.3	1.0	1.8	1.2	2.7

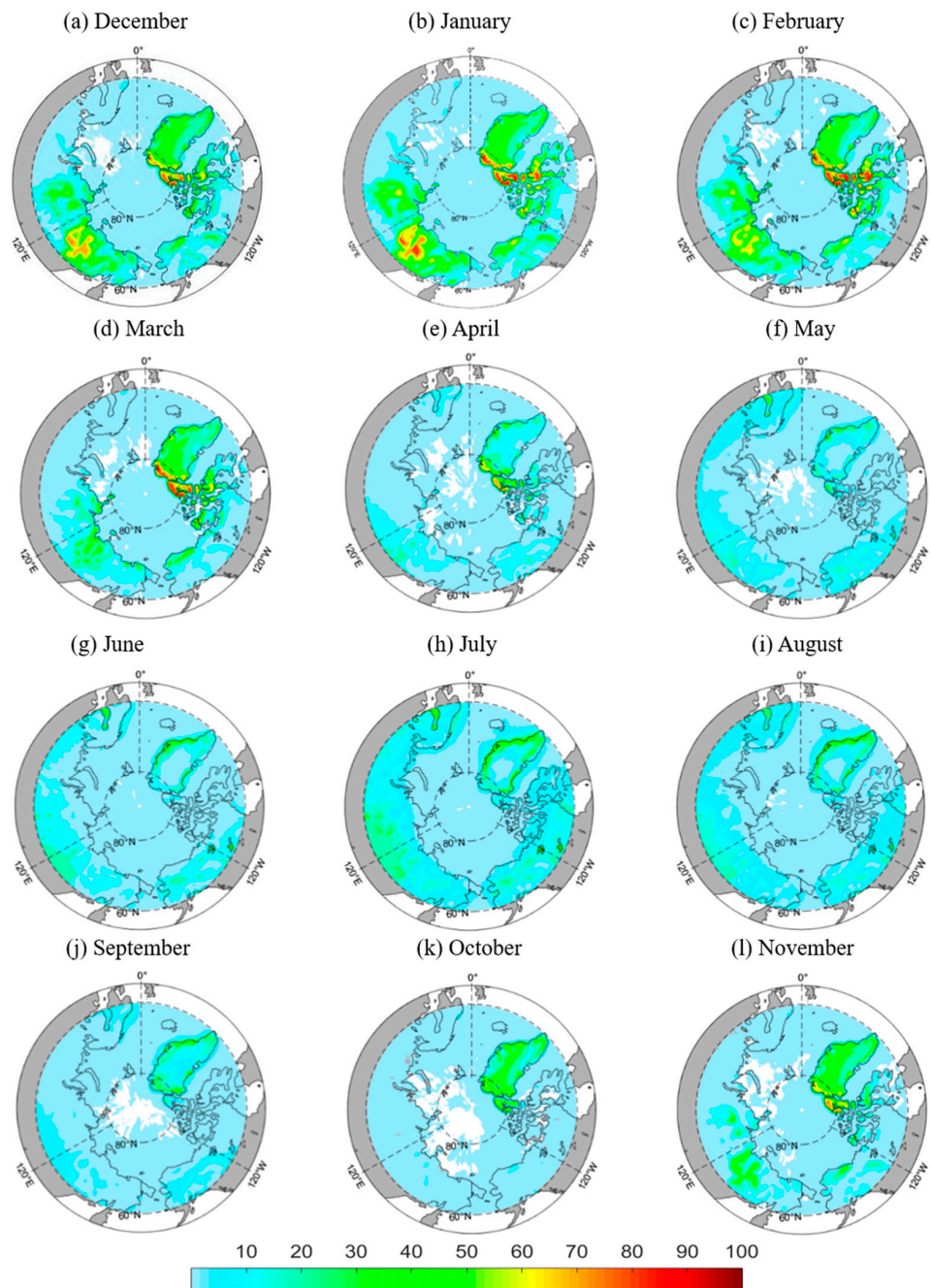


Figure 4. Monthly temporal and spatial distributions of total duct occurrence ratio in the Arctic. The color bar indicates the frequency of occurrences (unit: %).

In addition, atmospheric circulation and sea ice may also be connected to the seasonal and inter-annual fluctuations of atmospheric ducts. In Section 3.4, we will go into more detail about how atmospheric circulation and sea ice extent affect the frequency of atmospheric ducts.

Figures 5 and 6 show the spatial distribution of the monthly frequency of surface ducts and elevated ducts, respectively. The occurrences of surface and elevated ducts differ in frequency, but coincide in spatial distribution. Specifically, the frequency of surface ducts is greater than that of elevated ones (Table 1). The area with a high frequency of surface ducts is located in the coastal area, especially in the north and west of Greenland. Another area with more surface ducts is located northward of Eurasia in winter. The extremum center of the

elevated ducts is located on land, including Greenland and the northern part of the Eurasian continent. In the cold season, the extremum is more significant than in the warm season.

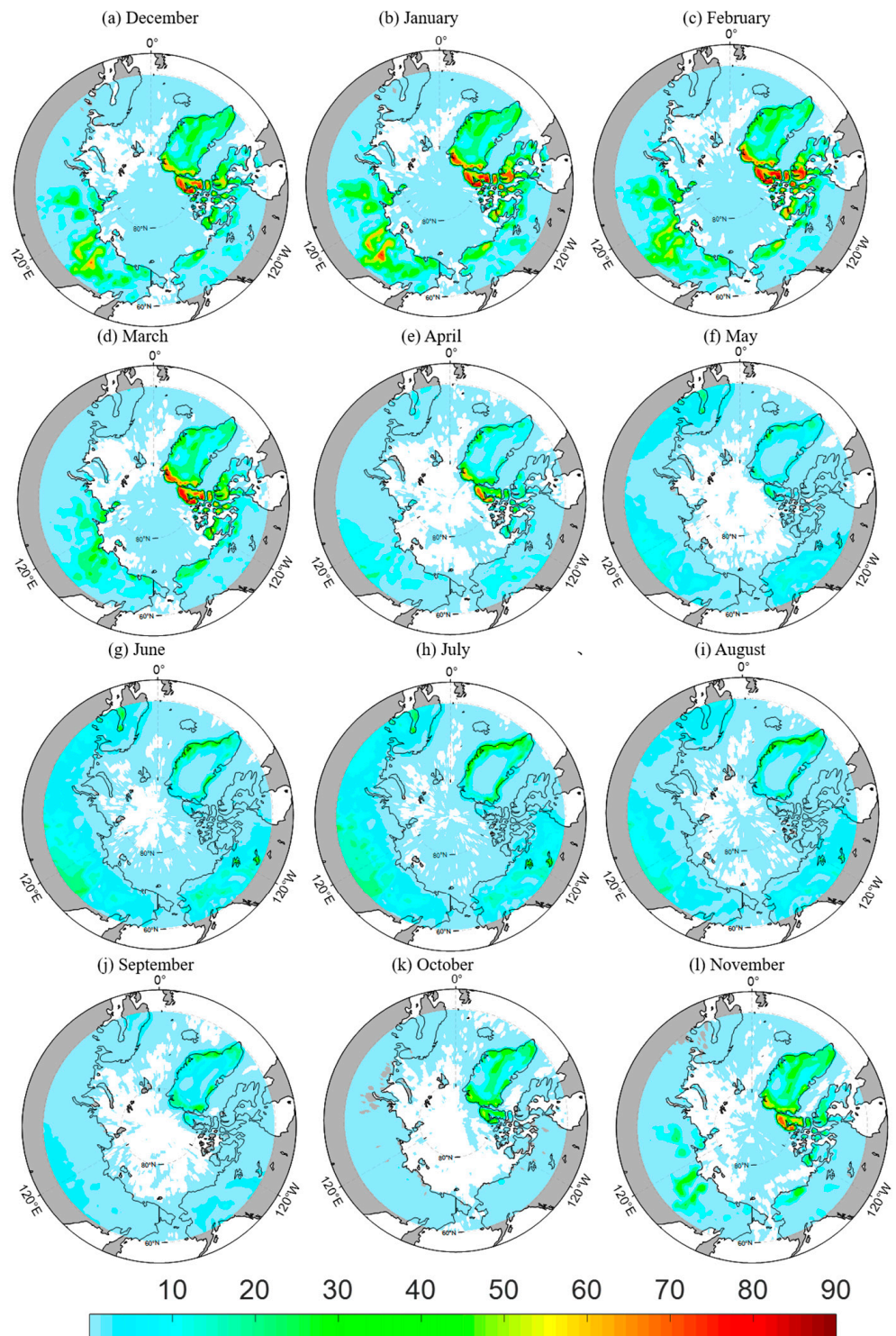


Figure 5. Monthly temporal and spatial distributions of surface duct occurrence ratio in the Arctic. The color bar indicates the frequency of occurrences (unit: %).

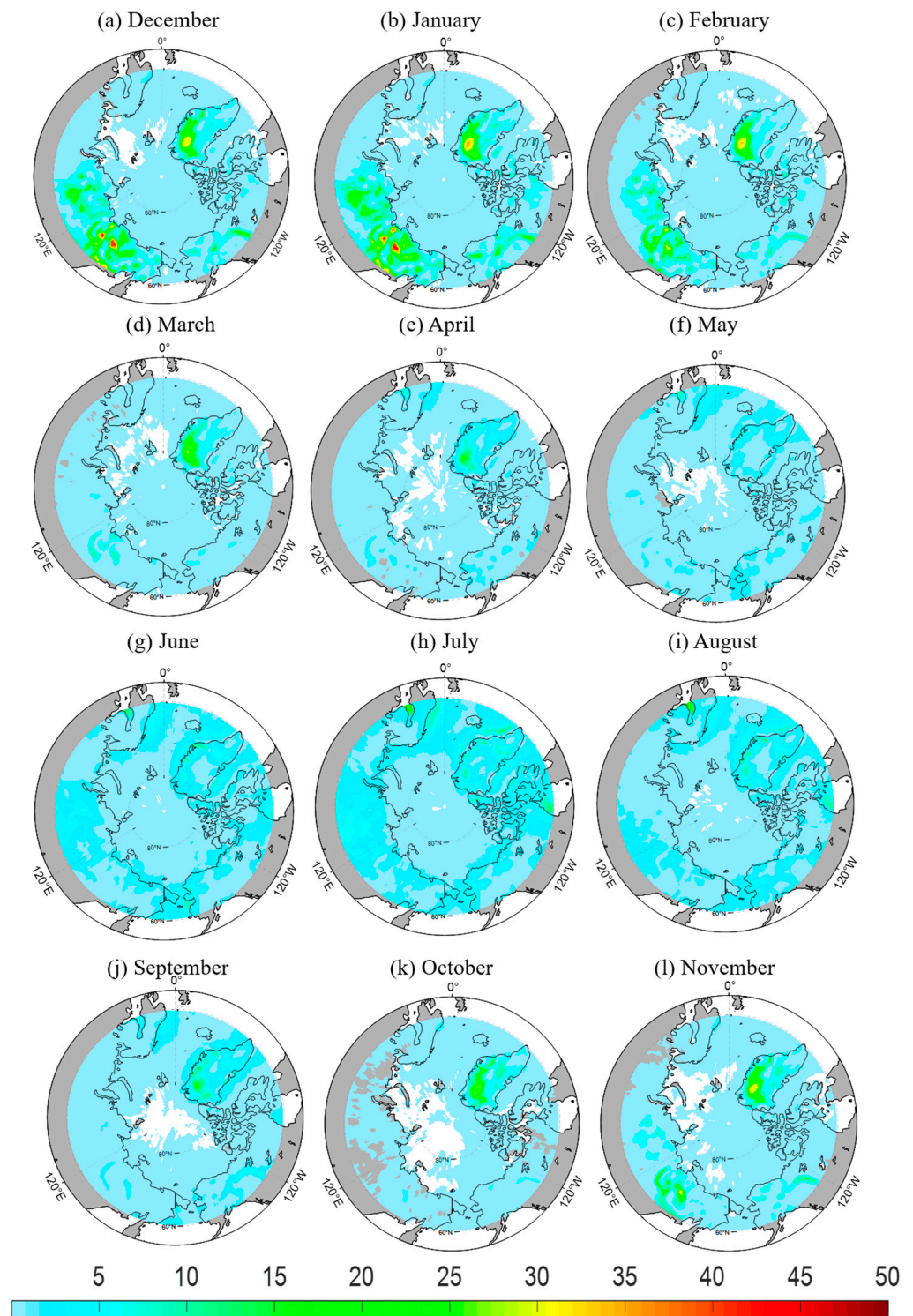


Figure 6. Monthly temporal and spatial distributions of elevated duct occurrence ratio in the Arctic. The color bar indicates the frequency of occurrences (unit: %).

3.3. Height and Intensity Characteristics of Atmospheric Ducts

3.3.1. Height Characteristics of Atmospheric Ducts

Figure 7 shows the frequency of the trapped layer thickness of surface ducts in each season (Figure 7a) and their monthly variation (Figure 7b). The results show that 60–80% of the layers are less than 100 m in each season, while 20–30% of the ducts are trapped in layers between 100 and 200 m. The trapped layers of the ducts that are more than 200 m

thick account for less than 5% in all seasons. The monthly average captured layer thickness of the surface ducts is shown in Figure 7b. The seasonal variation in surface duct thickness is not particularly obvious, only shown to be slightly larger in winter and summer than that in spring and autumn. The maximum layer is 75 m (± 35 m) in July and the minimum is 68 m (± 35 m) in April.

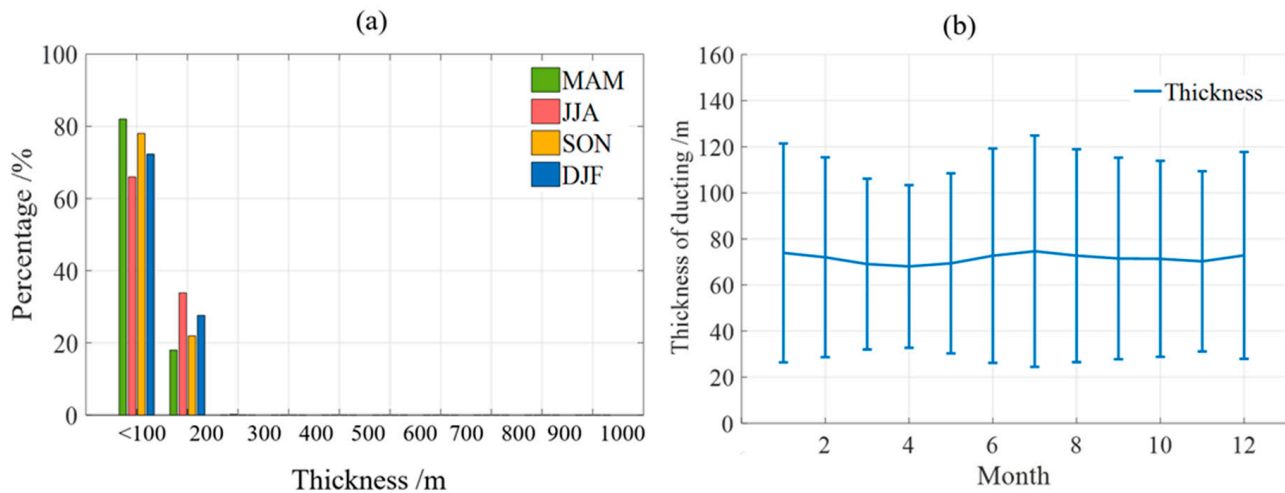


Figure 7. (a) Frequency of the trapped layer thickness of surface ducts in each season; (b) Monthly average thickness of surface trapped thickness (confidence level: 95%).

Figure 8 shows the seasonal frequency and monthly average changes of the trapped layer thickness (Figure 8a,b), bottom height (Figure 8c,d) and top height (Figure 8e,f) of the elevated ducts in the Arctic. The interval span of the trapped layer thickness (Figure 8a) is between 0 and 700 m, and more than 90% of it is less than 100 m, except in summer. The frequency of trapped layer thickness below 100 m is greater than that of the surface ducts, but the frequency above 200 m is also higher than that of the surface ducts. Figure 8c shows that the base height of the elevated ducts is between 30 and 600 m, but most ducts occur at a low height, and the frequency of the bottom height below 100 m is also above 90%, except in summer. In summer, not only is the trapped layer thickness of the elevated ducts thicker, but the bottom height of the ducts is also higher. Figure 8d shows the top height distribution of the elevated ducts. More than 85% of elevated ducts' top height are lower than 200 m.

The monthly variation of the trapped layer thickness of the elevated ducts is shown in Figure 8b. Combined with a thickness percentage of more than 100 m and the monthly variation of the thickness, the thickness of the elevated ducts in summer is slightly higher than that in other seasons. Seasonal variation of elevated ducts thickness is more obvious than that of the surface ducts. The average elevated trapped layer thickness in summer is 60 m (± 40 m), while that in the other months is 40 m (± 15 m). The captured layer thickness of the elevated ducts is lower than that of the surface ducts.

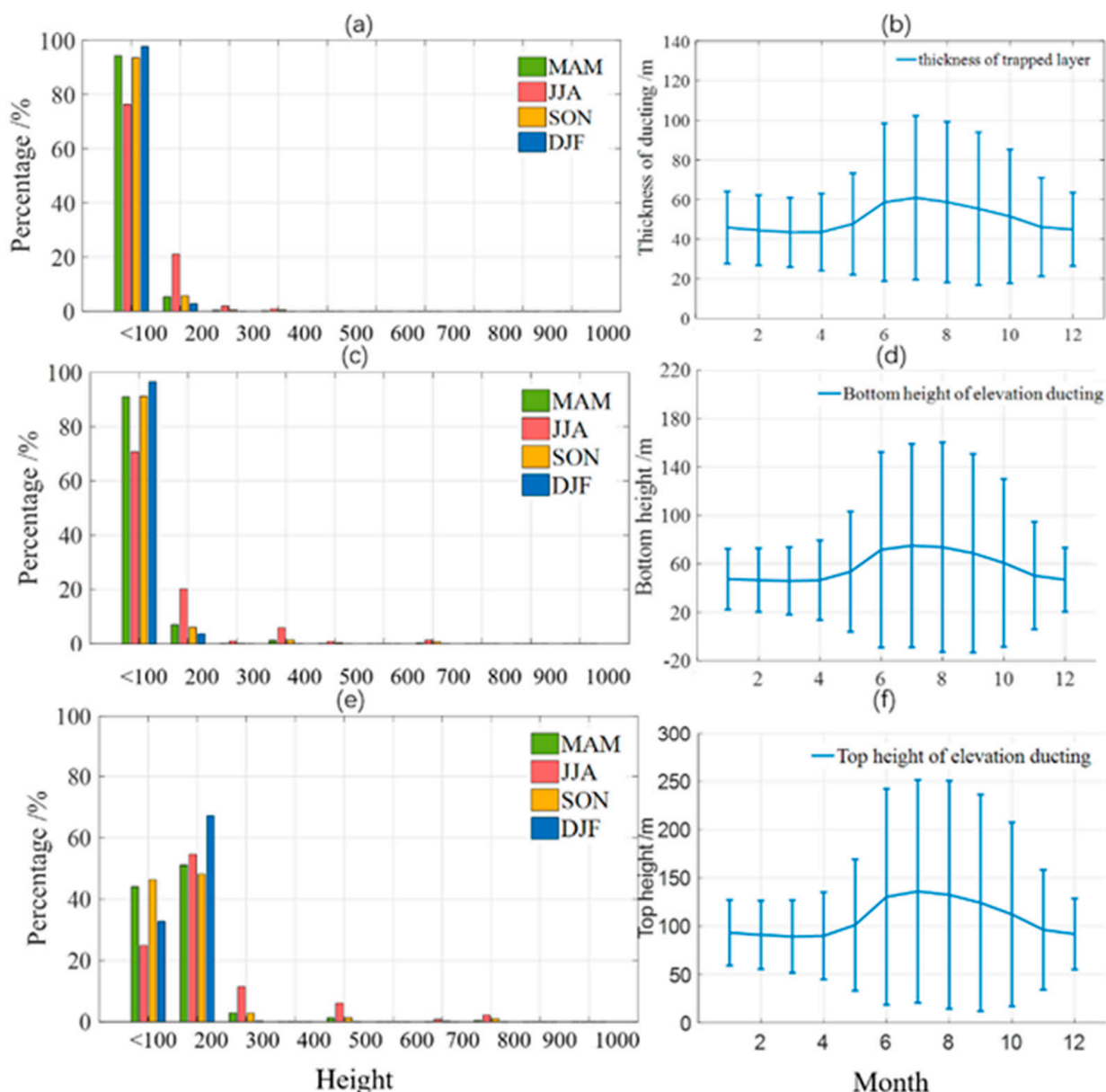


Figure 8. (a) Percentage of elevated trapped layer thickness; (b) Monthly average thickness of elevated trapped thickness (confidence level: 95%); (c) Percentage of bottom height of the elevated ducts; (d) Monthly average thickness of elevated bottom height (confidence level: 95%); (e) Percentage of bottom height of the elevated ducts; (f) Monthly average thickness of elevated top height (confidence level: 95%).

3.3.2. Statistics of Atmospheric Duct Intensities

The statistics of the total atmospheric duct intensities in each season are shown in Figure 9a. In general, the absolute value of atmospheric ducting strength greater than 10 M is considered a strong duct [19]. The frequency of a <1 M intensity in all seasons except winter is more than 30% in the Arctic, while the intensity of more than half of the ducts throughout the year is less than 3 M. The results show that the strength of ducts in Arctic is weak on average. Although the overall strength of ducts is weak, there are some strong events, albeit at a very low frequency. The frequency of strong ducts in winter is the greatest among all seasons, and the average intensity in winter is the strongest. This conclusion is also verified in Figure 9b, which shows the statistics of the monthly average intensity of different types of ducts, and also reflects two characteristics of intensity changes: 1. The

overall intensity of the elevated ducts is weaker than the surface ones. The annual average intensity of the elevated ducts ranges from 1.7 M (± 2 M) to 2.5 M (± 2.9 M), while the annual average intensity of the surface ducts ranges from 2.1 M (± 2.3 M) to 4.5 M (± 4.5 M). 2. The atmospheric duct intensity is strongest in winter, rather weak in spring and autumn, and slightly stronger in summer.

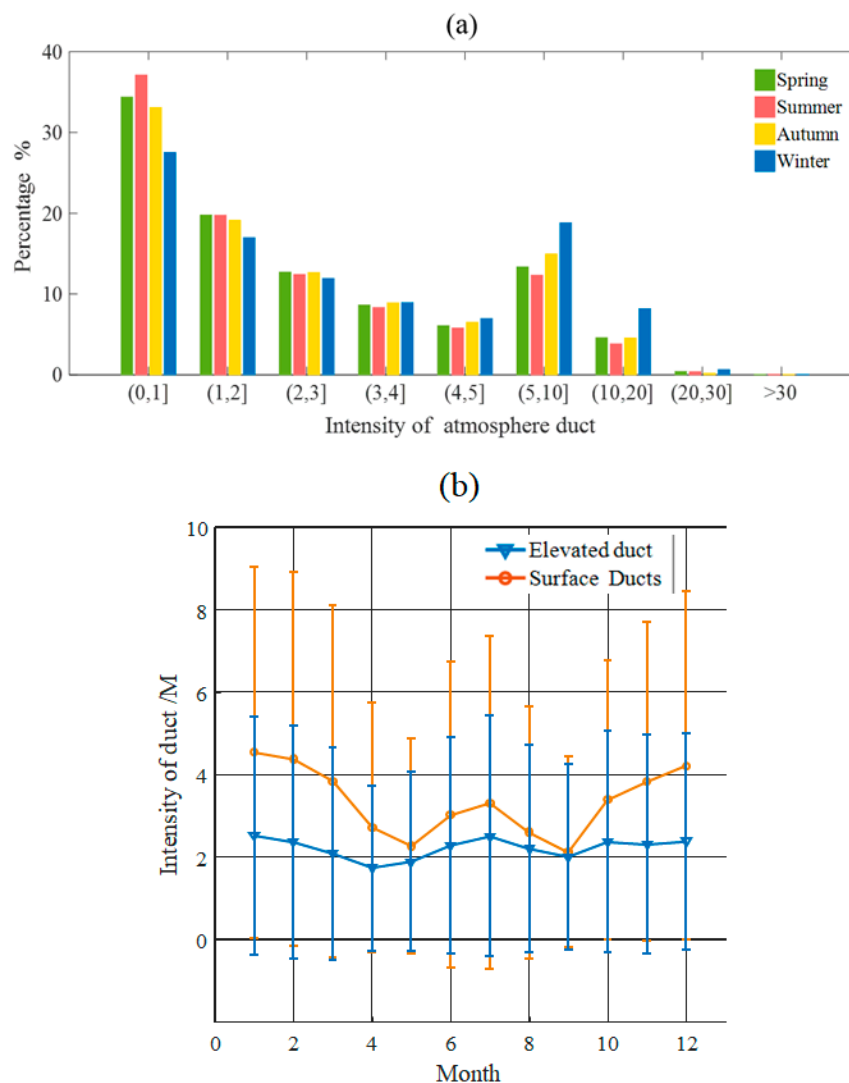


Figure 9. (a) Frequency of duct intensity in each season; (b) Statistics of the monthly average intensity of different types of ducts (unit: M).

The reason for the strongest atmospheric duct strength in the Arctic in winter is consistent with the cause of the number of atmospheric ducts discussed above, both of which are related to the enhancement of radiation inversion in the Arctic mainland. Based on the atmospheric sounding data of several coasts around the Arctic, Hao [20] found that the strength of the Arctic atmospheric duct is strongest in summer, followed by winter. This study shows that the intensity of ducts in winter is strongest, followed by summer. This difference mainly occurs because the former statistical data were concentrated on the coast observation, while the reanalysis data cover the whole Arctic. The results show that the increase in and enhancement of the Arctic atmospheric duct in winter mainly occurred in the continental region of the Arctic (60° N–70° N).

Summer is the most important period for navigation in the Arctic. The analysis of this study shows that the strength and number of ducts in this period are second only to those in winter. The changes during this period may be the combined influence of

permanent atmospheric activity centers, atmospheric circulation and seasonal variations in mesoscale weather systems in the middle to high latitudes and polar regions. Firstly, with the beginning of the warm season, the gradual strengthening of the Greenland high-pressure center triggers a sinking temperature inversion, which, as mentioned in the previous discussion, is the main cause of ducts on land mass. Secondly, there was more blocking activity high over the Asian continent, which carries large amounts of water and heat to the Arctic. In addition, there were also more cyclones entering the polar regions from middle and high latitudes in summer. These cyclones also transfer heat and water vapor to the polar regions [45]. The change in water vapor is closely related to the formation of ducts. These possible effects deserve further investigation.

3.3.3. Correlation between Atmospheric Duct Intensity and Trapped Layer Thickness

Next, the correlation coefficient between the trapped layer thickness and the intensity of the ducts is calculated, and the results are shown in Table 2. The results show that both the surface and elevated ducts have a positive correlation with the thickness of the trapped layer ($p < 0.05$). The positive correlation of surface ducts is more obvious than that of elevated ducts, especially in summer. This result indicates that the strength of the ducts is stronger when the trapped layer thickness of the duct is thicker.

Table 2. Correlation coefficient between the trapped layer thickness and intensity of atmospheric ducts (statistical significance at the 95% confidence level based on Student’s *t*-test).

Month	Correlation Coefficient (Surface)	Confidence Interval	Correlation Coefficient (Elevated)	Confidence Interval
1	0.230 *	0.229–0.231	0.256 *	0.254–0.257
	0.228 *	0.227–0.229	0.253 *	0.252–0.254
3	0.232 *	0.231–0.233	0.246 *	0.245–0.247
4	0.234 *	0.233–0.234	0.243 *	0.241–0.244
5	0.263 *	0.262–0.263	0.203 *	0.202–0.204
6	0.315 *	0.314–0.315	0.201 *	0.200–0.202
7	0.338 *	0.337–0.339	0.249 *	0.247–0.250
8	0.310 *	0.309–0.311	0.232 *	0.230–0.233
9	0.298 *	0.297–0.299	0.231 *	0.299–0.232
10	0.273 *	0.272–0.274	0.210 *	0.209–0.211
11	0.220 *	0.219–0.221	0.216 *	0.215–0.217
12	0.227 *	0.226–0.227	0.244 *	0.243–0.245

* represents $p < 0.05$.

3.4. Response of Atmospheric Ducts to AO and Sea Ice Extent

The occurrence of atmospheric ducts is related to the influence of the atmosphere and the underlying surface. The influence of the atmosphere includes small-scale sea and land winds, mesoscale and even synoptic-scale cyclones and anticyclones, along with changes in atmospheric circulation. The difference of underlying surface mainly includes the change of sea ice and land-sea discrepancy. Because the sea ice is melting, vessels can take advantage of channels in summer. Therefore, the relationship between the frequency of ducts in summer and the atmospheric circulation and sea ice were studied. Both the Arctic Oscillation (AO) index and sea ice extent for the period of 1989–2018 are standardized in this paper. Figure 10 shows the standardized AO index in summer and the average sea ice extent in September. September is the month of the year with the lowest Arctic sea ice extent, and this is a reflection of how much ice retreated that year. The sea ice extent in summer has declined significantly over the last 30 years ($p < 0.05$).

It can be seen from Figure 11a that the correlation between the AO and atmospheric ducting basically exhibits zonal distribution. There is a negative correlation between the frequency of atmospheric ducts and the AO in most regions north of 75° N, except in eastern Greenland and northern Russia. A positive correlation between the frequency of atmospheric ducts and the AO in most regions in the range of 60–75° N, including northern and central

Canada, eastern Greenland, northern Russia and other regions ($p < 0.05$). However, there are interruption regions in the positive latitudinal belt, which show negative correlations, including the Alaska and Greenland ($p < 0.05$) regions. The northern side of Greenland and the central and northern parts and the coast of Russia are the main duct occurrence regions, and these regions are significantly correlated with the AO ($p < 0.05$).

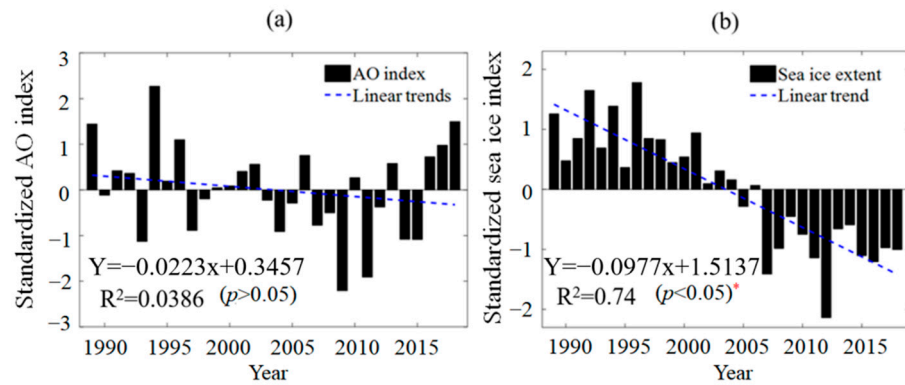


Figure 10. Time series of standardized AO index in summer and sea ice extent index in September: (a) AO; (b) sea ice extent. The blue dashed line is the trend (statistical significance at the 95% confidence level based on Student’s *t*-test, * represents $p < 0.05$).

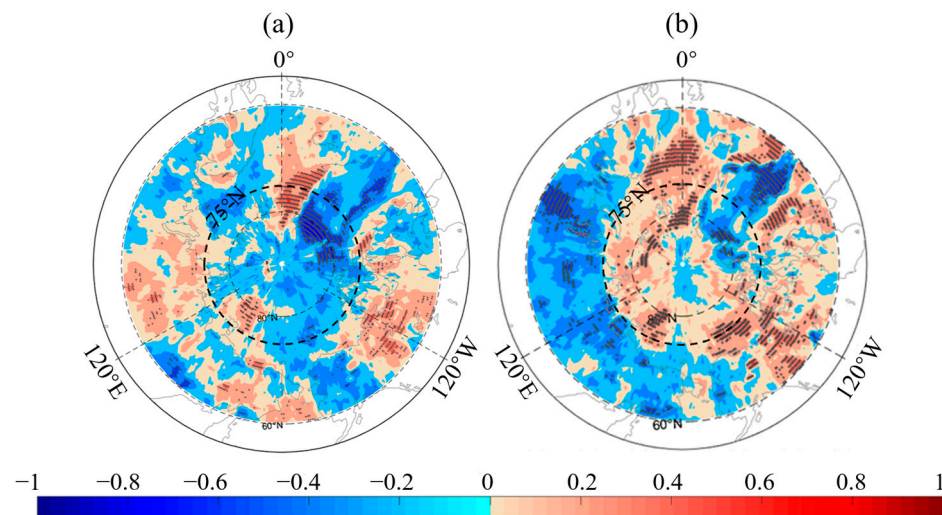


Figure 11. Correlation coefficients between atmosphere duct density and AO/sea ice extent index for the same season during the period of 1989–2018 in summer: (a) AO; (b) sea ice. The black dots denote that the linear trend is significant at 95%.

The correlation between the sea ice extent and atmospheric ducts in summer is mainly negative in land areas (Figure 11b), but only that in the northwestern parts of Greenland and Russia is obvious ($p < 0.05$). On the contrary, the Arctic Ocean (floating ice area) is positively correlated, especially in the outer floating ice area around 75–80° N, including the north of Russia, Canada and the Greenland Sea ($p < 0.05$). The change in Arctic sea ice will affect the formation and intensity of the radiation inversion layer in the Arctic atmosphere [35]. In the dense ice area, it is easier for an inversion layer to form than in open water, and the inversion is closely related to the formation of atmospheric ducting. Therefore, it is speculated that the positive correlation between atmospheric ducting and the sea ice extent in the Arctic Ocean is related to the change in radiation inversion caused by sea ice change, but it still needs further study.

To further explain the relationship between the AO and ducting, the anomaly of the 500 hPa height field, the sea level pressure, the surface wind speed at 10 m and the duct

counts in summer corresponding to the positive (>0.6 standard deviation) and negative (<-0.6 standard deviation) of the AO were analyzed (Figure 12). The positive and negative abnormal years of the AO are shown in Table 3. Completely opposite effects occur in the 500 hPa height, sea level pressure, surface wind speed and duct counts in the Arctic in different anomaly AO years. In the positive (negative) abnormal years of AO, the polar vortex is stronger (weaker), the sea level pressure is lower (higher), and the wind speed in the Arctic Ocean region increases (decreases), and then the duct counts decrease (increase). It is found in Figure 12(a-1,a-2) that when the AO index is positive, the positive anomaly area of the wind speed basically corresponds to the ducting decrease area, including the Arctic Ocean, northern Greenland, and the Barents Sea. The negative anomaly area of wind speed basically corresponds to the ducting increase area, including northeast Russia, the northern coast of Canada and northern Greenland and so on (Figure 12(b-1,b-2)). This also shows that the AO affects the frequency of atmospheric duct generation through the anomaly of surface wind speed in different phases.

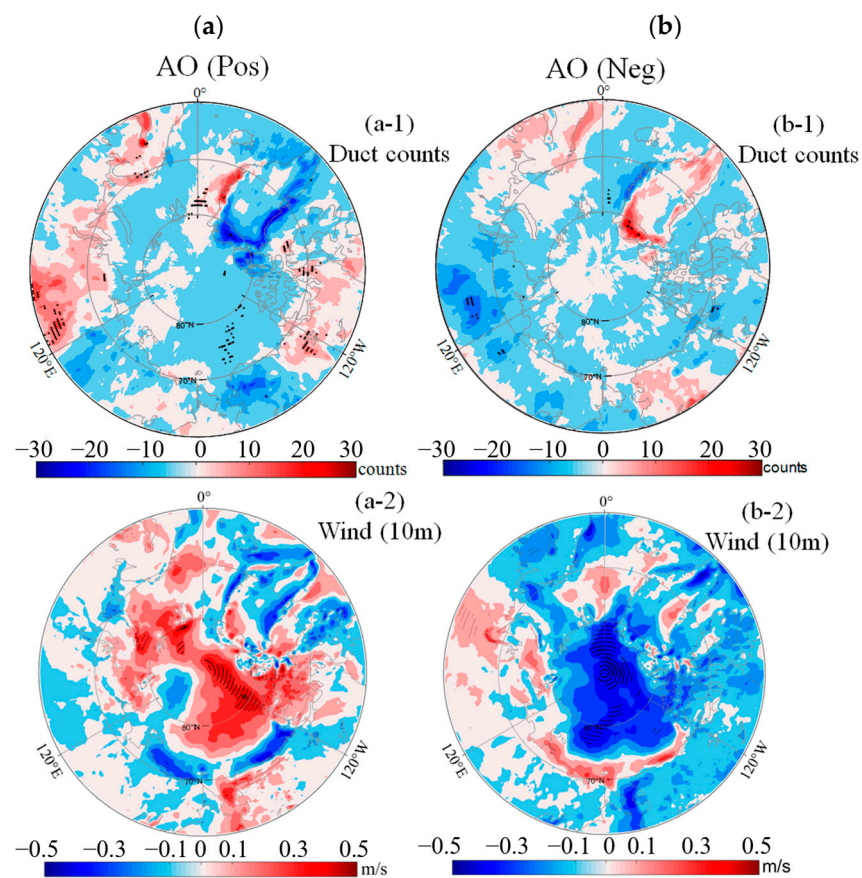


Figure 12. Cont.

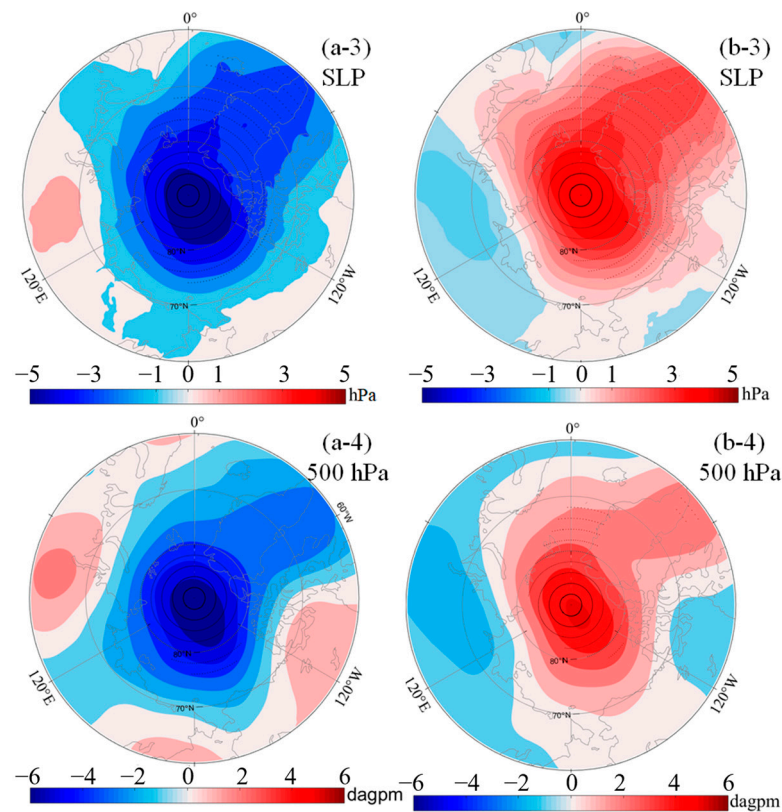


Figure 12. Composite of 500 hPa geopotential height anomaly, sea level pressure anomaly, 10 m wind speed anomaly and duct counts anomaly during the positive (a) anomalous (AO index > 0.6 standard deviation) and negative; (b) anomalous (normalized AO index < −0.6 standard deviation) years of AO in summer. Black dots indicate that the value is significant at 95% based on Student's *t*-test.

Table 3. Positive and negative abnormal years of AO.

Positive AO anomaly years	1989, 1994, 1996, 2006, 2016, 2017, 2018
Negative AO anomaly years	1993, 1997, 2004, 2007, 2009, 2011, 2014, 2015

The positive phase of the AO corresponds to the very large cold vortex over the North Pole, and leads to a flat-zonal, strong westerly circulation in the mid-latitudes, with less fluctuation in extratropical cyclones and other synoptic scales. The polar cyclone activity moves north [45]. Affected by the polar cyclones, sea level pressure shows a negative anomaly and wind speed shows a positive anomaly in the Arctic Ocean, which is consistent with the analysis results in Figure 12. This situation is not conducive to the generation of ducting in the Arctic Ocean. However, it is advantageous for ducts near the range of 60–75° N in the continent region. On the contrary, the Arctic Ocean is often occupied by surface high pressure or the upper air anti-cyclonic, while the mid-latitude circulation fluctuation amplitude increases, the westerly belt becomes weak, and the blocking high pressure easily forms. The north–south exchange of warm and cold air is intense, and the wind force increases (Figure 12(b-2)), which is not conducive to the formation of atmospheric ducts in the 60–75° N zone.

4. Conclusions and Discussions

This study used the ERA-Interim reanalysis data from 1989 to 2018 to calculate the frequency, thickness, intensity and variation of different types of atmospheric ducts in the Arctic, and to further analyze the response of Arctic atmospheric ducts to atmospheric circulation and the Arctic Sea ice extent.

The results show that the frequency of the total atmospheric ducts is less than 10%, the frequency of the surface ducts is two to three times higher than the elevated ducts, and the high-frequency region is consistent with the previous results of several sounding observation stations around the continent in the polar region [20]. Although the frequency of atmospheric ducts in the Arctic is relatively low, the spatial and seasonal differences in their frequency are obvious, and the high-frequency region of the ducts can exceed 80%.

Previous studies have shown that land radiative cooling is conducive to the occurrence of land atmospheric ducts. With the increase in latitude, the land area in the Arctic decreases. Our research results also show that atmospheric ducting has a lower frequency in the Arctic Ocean compared to the continental landmass, which also corresponds to the radiation difference between land and ocean. At the same time, the high-frequency region of the atmospheric ducts is mainly located on the coast of the Arctic and at a great height inland, especially in the coastal area of northwestern Greenland and the inland plateau area of the Arctic, including the Central Siberian Plateau of northern Russia, the Chersky Plateau and the Yukon Plateau of northern Alaska. In general, the seasonal differences in the occurrence frequency of atmospheric ducts are generally higher in winter and spring and lower in summer and autumn, but in the Arctic continent, summer is second only to winter.

The thickness of the trapped layer of ducts is generally low, with more than 90% being below 100 m. In winter and summer, the thickness of the surface ducts is thicker, while that of the elevated ducts is thicker in summer. The thickness of the elevated ducts is less than that of the surface ducts. The intensity of the ducts is generally weak. The average intensity of the surface ducts ranges from 1.7 M (± 2 M) to 2.5 M (± 2.9 M), and the average intensity of the elevated ducts ranges from 2.1 M (± 2.3 M) to 4.5 M (± 4.5 M), which is lower than that of the surface ducts. The intensity of the ducts is stronger in winter, and weaker in spring and autumn. There is a positive correlation between the intensity of the two duct types and the thickness of the trapped layer, especially for the surface ducts in summer.

The relationship between the frequency of the Arctic atmospheric ducts in summer and atmospheric circulation and the sea ice extent was further analyzed. The AO affects the surface wind force in the Arctic. The variation in wind speed near the ground has a direct influence on the formation of ducting. A weakening wind speed is beneficial to the formation and maintenance of ducting, while a stronger wind speed is unfavorable. When the AO is in positive (negative) phase, the surface wind speed of the central Arctic Ocean increases (decreases) and the frequency of the atmospheric ducts there decreases (increases). On the contrary, the surface wind speed of some regions in 60–75° N decreases (increases) and the frequency of the atmospheric ducts shows an increasing (decreasing) trend, including in northeast Russia, the northern coast of Canada and northern Greenland.

From 1989 to 2018, the Arctic Sea ice extent decreased significantly. Accompanied by the decrease in the sea ice extent, the number of atmospheric ducts in the Arctic Ocean also decreased, and the decrease in atmospheric ducts in the floating ice area was more significant than that in the dense ice area. On the contrary, the number of continental and coastal atmospheric ducts in the Arctic region increased during this time, and significantly in some regions, including the main regions of the Arctic ducts, such as northern Greenland and central Russia. It is thus preliminarily concluded that the sea–land difference in the atmospheric duct variation in the Arctic is related to the change in the atmospheric boundary layer and radiation characteristics caused by the decrease in the sea ice extent.

The results of this study will provide a reference for the detection and application of the Arctic atmospheric ducts and the improvement of prediction and diagnosis systems. However, the reasons underlying changing atmospheric duct characteristics in the Arctic require further analysis.

Author Contributions: Conceptualization, T.Q. and B.S.; methodology, L.C. and J.Y.; validation, J.Y.; formal analysis, T.Q. and J.Y.; investigation, T.Q. and B.S.; data curation, T.Q., H.S., J.M. and W.Y.; writing—original draft preparation, T.Q.; writing—review and editing, T.Q. and J.Y.; supervision, B.S.; funding acquisition, B.S. All authors have read and agreed to the published version of the manuscript.

Funding: This research was funded by the Key Basic Research Projects of Basic Strengthening Plan of China (Grant no. 2020-JCJQ-ZD-268-00), National Natural Science Foundation of China (Joint Meteorological Foundation) (Grant no. U2242206) and the National Natural Science Foundation of China (Grant no. 42174192).

Institutional Review Board Statement: Not applicable.

Informed Consent Statement: Not applicable.

Data Availability Statement: Not applicable.

Acknowledgments: The GPS radiosonde data used in this paper were taken from the sixth to ninth Chinese Arctic scientific expeditions, and we graciously thank the members of the expeditions for their assistance.

Conflicts of Interest: The authors declare no conflict of interest.

References

1. Serreze, M.C.; Barry, R.G. Processes and impacts of Arctic amplification: A research synthesis. *Glob. Planet.* **2011**, *77*, 85–96. [[CrossRef](#)]
2. Sporyshev, P.V.; Kattsov, V.M.; Gulev, S.K. Changes in surface temperature in the Arctic: Reliability of model reproduction and probabilistic forecast for the near future. *Dokl. Earth Sci.* **2018**, *479*, 503–506. [[CrossRef](#)]
3. Aksenov, Y.; Popova, E.E.; Yool, A.; Nurser, A.G.; Williams, T.D.; Bertino, L.; Bergh, J. On the future navigability of Arctic sea routes: High-resolution projections of the Arctic Ocean and sea ice. *Mar. Policy.* **2017**, *75*, 300–317. [[CrossRef](#)]
4. Oh, J.; Yang, S.; Lee, B.L. Future projections of ship accessibility for the Arctic Ocean based on IPCC CO₂ emission scenarios. *Asia-Pac. J. Atmos. Sci. Vol.* **2017**, *53*, 43–50. [[CrossRef](#)]
5. Pustovalov, K.N.; Kharyutkina, E.V.; Korolkov, V.A.; Nagorskiy, P.M. Variations in Resources of Solar and Wind Energy in the Russian Sector of the Arctic. *Atmos. Ocean. Opt.* **2020**, *33*, 282–288. [[CrossRef](#)]
6. Zuev, V.V.; Savelieva, E.S.; Pavlinsky, A.V. Features of Stratospheric Polar Vortex Weakening Prior to Breakdown. *Atmos. Ocean. Opt.* **2022**, *35*, 183–186. [[CrossRef](#)]
7. Kovadlo, P.G.; Shikhovtsev, A.Y.; Yazev, S.A. The Role of Glaciers in the Processes of Climate Warming. *Atmos. Ocean. Opt.* **2022**, *35*, 434–438. [[CrossRef](#)]
8. Lopez, P. A 5-yr 40-km-Resolution Global Climatology of Superrefraction for Ground-Based Weather Radars. *J. Appl. Meteorol. Clim.* **2009**, *48*, 89–110. [[CrossRef](#)]
9. Patterson, W.L. *Climatology of Marine Atmospheric Refractive Effects. A Compendium of the Integrated Refractive Effects Prediction System (IREPS) Historical Summaries*; Naval Ocean Systems Center: San Diego, CA, USA, 1982.
10. Babin, S.M. Surface Duct Height Distributions for Wallops Island, Virginia, 1985–1994. *J. Appl. Meteorol.* **1996**, *35*, 86–93. [[CrossRef](#)]
11. Huang, L.; Zhao, X.; Liu, Y. The Statistical Characteristics of Atmospheric Ducts Observed Over Stations in Different Regions of American Mainland Based on High-Resolution GPS Radiosonde Soundings. *Front. Environ. Sci.* **2022**, *10*, 946226. [[CrossRef](#)]
12. Mai, Y.; Sheng, Z.; Shi, H.; Liao, Q.; Zhang, W. Spatiotemporal Distribution of Atmospheric Ducts in Alaska and Its Relationship with the Arctic Vortex. *Int. J. Antennas Propag.* **2020**, *2020*, 9673289. [[CrossRef](#)]
13. Liu, C.G.; Huang, J.Y.; Jiang, C.Y. The appearance of the atmospheric ducts structure in the troposphere over the southeast coast. *Chin. J. Radio Sci.* **2002**, *17*, 509–513. (In Chinese)
14. Ding, J.; Fei, J.; Huang, X.; Cheng, X.; Hu, X. Observational occurrence of tropical cyclone ducts from GPS dropsonde data. *J. Appl. Meteorol. Climatol.* **2013**, *52*, 1221–1236. [[CrossRef](#)]
15. Cheng, G.; Gao, Z.; Zheng, Y.; Dai, C.; Zhou, M. A Study on Low-level Jets and Temperature Inversion over the Arctic Ocean by Using SHEBA Data. *Clim. Environ. Res.* **2013**, *18*, 23–31. (In Chinese)
16. Cheng, Y.H.; Zhao, Z.W.; Zhang, Y.S. Statistical analysis of low-altitude atmospheric ducts over the South China Sea during monsoon. *Chin. J. Radio Sci.* **2012**, *27*, 268–274. (In Chinese)
17. Chen, L.; Gao, S.H.; Kang, S.F.; Zhang, Y.S.; Wu, Z.M. Statistical analysis on spatial-temporal features of atmospheric ducts over chinese regional seas. *Chin. J. Radio Sci.* **2009**, *24*, 702–708.
18. Cheng, Y.H.; Yang, X.K.; Zhang, Y.S. Characteristics over the China sea based on ECMWF reanalysis data. *Oceanol. Limnol. Sin.* **2021**, *52*, 11. (In Chinese)
19. Wang, H.; Ma, B.; Jiao, L. Study on the distribution of atmospheric ducts based on ECMWF reanalysis data. *J. Meteorol.* **2021**, *79*, 521–530. (In Chinese) [[CrossRef](#)]
20. Hao, X.J.; Li, Q.L.; Guo, L.X. Spatial and temporal characteristics of the atmosphere ducts over the North Pole. *Chin. J. Polar Res.* **2018**, *30*, 349. (In Chinese)
21. Von Engeln, A. A ducting climatology derived from the European Centre for Medium-Range Weather Forecasts global analysis fields. *J. Geophys. Res. Atmos.* **2004**, *109*, D18104. [[CrossRef](#)]
22. Mentés, S.; Kaymaz, Z. Investigation of Surface Duct Conditions over Istanbul, Turkey. *J. Appl. Meteorol. Clim.* **2007**, *46*, 318–337. [[CrossRef](#)]

23. Murthy, N.R.K.; Rao, S.V.B. Study on the occurrence of duct and super-refraction over Indian region. *Int. J. Curr. Res. Rev.* **2013**, *5*, 12–20.
24. Fei, J.; Ding, J.; Huang, X.; Cheng, X.; Hu, X. Numerical study on the impacts of the bogus data assimilation and sea spray parameterization on typhoon ducts. *J. Meteorol. Res.* **2013**, *27*, 308–321. [[CrossRef](#)]
25. Liang, Z.; Ding, J.; Fei, J.; Cheng, X.; Huang, X. Maintenance and Sudden Change of a Strong Elevated Ducting Event Associated with High Pressure and Marine Low-Level Jet. *J. Meteorol. Res.* **2020**, *34*, 1287–1298. [[CrossRef](#)]
26. Manjula, G.; Raman, M.R.; Ratnam, M.V.; Chandrasekhar, A.V.; Rao, S.V.B. Diurnal variation of ducts observed over a tropical station, Gadanki, using high-resolution GPS radiosonde observations. *Radio Sci.* **2016**, *51*, 247–258. [[CrossRef](#)]
27. Wei, L.; Peitao, Z.; Qiyun, G.; Mian, W. The international radiosonde intercomparison results for China-made GPS radiosonde. *J. Appl. Meteorol. Sci.* **2011**, *22*, 453–462.
28. Dee, D.P.; Uppala, S. Variational bias correction of satellite radiance data in the ERA-Interim reanalysis. *Q. J. R. Meteorol. Soc.* **2009**, *135*, 1830–1841. [[CrossRef](#)]
29. Graham, R.M.; Hudson, S.R.; Maturilli, M. Improved performance of ERA5 in Arctic gateway relative to four global atmospheric reanalysis. *Geophys. Res. Lett.* **2019**, *46*, 6138–6147. [[CrossRef](#)]
30. Bromwich, D.H.; Wilson, A.B.; Bai, L.S.; Moore, G.W.; Bauer, P. A comparison of the regional Arctic System Reanalysis and the global ERA—Interim Reanalysis for the Arctic. *Q. J. R. Meteorol. Soc.* **2016**, *142*, 644–658. [[CrossRef](#)]
31. Dee, D.P.; Uppala, S.M.; Simmons, A.J.; Berrisford, P.; Poli, P.; Kobayashi, S.; Andrae, U.; Balmaseda, M.A.; Balsamo, G.; Bauer, P.; et al. The ERA-Interim reanalysis: Configuration and performance of the data assimilation system. *Q. J. R. Meteorol. Soc.* **2011**, *137*, 553–597. [[CrossRef](#)]
32. Berrisford, P.; Dee, D.; Poli, P.; Brugge, R.; Fielding, K.; Fuentes, M.; Kallberg, P.; Kobayashi, S.; Uppala, S.; Simmons, A. The ERA-Interim Archive Version 2.0. ERA Report Series 1. 2011. Available online: <http://www.ecmwf.int/en/elibrary/8174-era-interim-archive-version-20> (accessed on 2 October 2022).
33. Thompson, D.W.J.; Wallace, J.M. Annular modes in the extratropical circulation. Part I: Month-to-month variability. *J. Clim.* **2000**, *13*, 1000–1016. [[CrossRef](#)]
34. Hersbach, H.; Bell, B.; Berrisford, P.; Biavati, G.; Horányi, A.; Muñoz Sabater, J. ERA5 monthly averaged data on single levels from 1959 to present. Copernicus Climate Change Service (C3S). *Clim. Data Store* **2019**, *10*, 252–266.
35. Tian, Z.; Zhang, D.; Song, X.; Zhao, F.; Li, Z.; Zhang, L. Characteristics of the atmospheric vertical structure with different sea ice covers over the Pacific sector of the Arctic Ocean in summer. *Atmos. Res.* **2020**, *245*, 105074. [[CrossRef](#)]
36. Xie, Q.; Huang, K.; Wang, D.; Yang, L.; Chen, J.; Wu, Z.; Li, D.; Liang, Z. An inter-comparison of GPS radiosonde soundings during the eastern tropical Indian Ocean experiment. *Acta Oceanol. Sin.* **2014**, *33*, 127–134. [[CrossRef](#)]
37. Bean, B.R.; Dutton, E.J. *Radio Meteorology*; Dover: New York, NY, USA, 1968; 435p.
38. Lee, W.; Song, I.; Kim, J.; Kim, Y.H.; Jeong, S.; Eswarajah, S.; Murphy, D.J. The Observation and SD-WACCM Simulation of Planetary Wave Activity in the Middle Atmosphere During the 2019 Southern Hemispheric Sudden Stratospheric Warming. *J. Geophys. Res. Space Phys.* **2021**, *126*, e2020JA029094. [[CrossRef](#)]
39. Rogers, R.R.; Yau, M.K. *A Short Course in Cloud Physics*, 3rd ed.; Pergamon Press: London, UK, 1989.
40. Bolton, D. The Computation of Equivalent Potential Temperature. *Mon. Weather Rev.* **1980**, *108*, 1046–1053. [[CrossRef](#)]
41. Liu, J.W.; Guo, H.; Li, Y.D. *Basic Calculation of Physical Quantities for Weather Analysis and Forecast*; China Meteorological Press: Beijing, China, 2005. (In Chinese)
42. Turton, J.D.; Bennetts, D.A.; Farmer, S.F.G. An introduction to radio Ducting. *Meteor Mags* **1988**, *117*, 245–254.
43. Ruman, C.J.; Monahan, A.H.; Sushama, L. Climatology of Arctic temperature inversions in current and future climates. *Theory Appl. Climatol.* **2022**, *150*, 121–134. [[CrossRef](#)]
44. Shikhovtsev, A.Y.; Bolbasova, L.A.; Kovadlo, P.G.; Kiselev, A.V. Atmospheric parameters at the 6-m Big Telescope Alt-azimuthal site. *Mon. Not. R. Astron. Soc.* **2020**, *493*, 723–729. [[CrossRef](#)]
45. Wei, L.X.; Qin, T.; Li, C. Seasonal and inter-annual variations of Arctic cyclones and their linkage with Arctic sea ice and atmospheric teleconnections. *Acta Oceanol. Sin.* **2017**, *10*, 5–11. [[CrossRef](#)]